INTERNATIONAL JOURNAL FOR NUMERICAL METHODS IN ENGINEERING
Int. J. Numer. Meth. Engng 2009; **77**:536–557
Published online 22 July 2008 in Wiley InterScience (www.interscience.wiley.com). DOI: 10.1002/nme.2424

Integration-free Coons macroelements for the solution of 2D Poisson problems

C. G. Provatidis*, †

School of Mechanical Engineering, National Technical University of Athens, 9 Heroon Polytechniou Avenue, Zografou Campus, GR-157 73 Athens, Greece

SUMMARY

Large isoparametric macroelements with closed-form cardinal global shape functions under the label 'Coons-patch macroelements' (CPM) have been previously proposed and used in conjunction with the finite element method and the boundary element method. This paper continues the research on the performance of CPM in conjunction with the collocation method. In contrast to the previous CPM that was based on a Galerkin/Ritz formulation, no domain integration is now required, a fact that justifies the name 'integration-free Coons macroelements'. Therefore, in addition to avoiding mesh generation, and saving human effort, the proposed technique has the additional advantage of further reducing the computer effort. The theory is supported by five test cases concerning Poisson and Laplace problems within 2D smooth quadrilateral domains. Copyright © 2008 John Wiley & Sons, Ltd.

Received 1 June 2007; Revised 20 May 2008; Accepted 10 June 2008

KEY WORDS: finite elements; transfinite interpolation; global approximation; boundary-value problems; global collocation

1. INTRODUCTION

The numerical solution of boundary-value problems (BVP) has been an open issue for over a century. The *global* approximation character of the early Rayleigh/Ritz methods [1] was later replaced by several finite element schemes applicable to arbitrary domains thanks to their *local* approximation ability [2]. Despite that, the latter advantage created the need for a high manual

*Correspondence to: C. G. Provatidis, School of Mechanical Engineering, National Technical University of Athens, 9 Heroon Polytechniou Avenue, Zografou Campus, GR-157 73 Athens, Greece.
†E-mail: cprovat@central.ntua.gr, URL: http://users.ntua.gr/cprovat

effort for data preparation, an issue strongly related to the mesh generation. Therefore, many efforts aimed at reducing the mesh generation activities by using large elements have appeared. Among them could be mentioned the rational/polygonal finite element methods [3, 4], boundary element methods [5], Trefftz and other boundary methods [6, 7], meshfree and meshless techniques [8, 9], as well as CAD-oriented techniques using NURBS [10–12].

In the context of the abovementioned CAD-oriented techniques, the author has contributed by applying the Coons–Gordon transfinite mapping in conjunction with the finite element method [13] and the boundary element method [14, 15]. It is to be noted that Coons–Gordon interpolation is the precursor of the well-known Bézier and NURBS computer-aided design surfaces [16]. Although the analysis of 3D structures is of major engineering interest [13, 17, 18], for reasons of simplicity the investigation on the performance of the Coons' method initiated from 2D domains [19]. In more detail, large *isoparametric* macroelements with closed-form cardinal global shape functions were developed under the label '*Coons-patch macroelements*' (CPM). It was found that for some particular problems the boundary-only Coons' interpolation (Appendix A) could approximate the solution with adequate accuracy [19–22] while internal nodes in general had to be added in order to achieve convergence [23]. Furthermore, it was found that the internal nodes could be located at different positions from those dictated by the boundary ones, while the most complex domains in which the CPM was successfully applied so far were of a Π-like shape [24–26]. Another interesting finding was that, in the particular case of using Lagrange interpolation along each of the four sides of the patch, the boundary-only Coons macroelement coincides with the well-known *Serendipity* type, while in the case of internal nodes being at the same location with the boundary nodes it coincides with the well-known *Lagrangian* type finite element [24–26]. Apart from the aforementioned Lagrange polynomials, a CPM could be also formulated in conjunction with cubic B-splines [19], piecewise-linear [20, 21], as well as other types of interpolation such as Bézier (Bernstein polynomials), higher order B-splines, and NURBS [10] along each of the four sides of the patch.

In spite of the above advantages, the treatment of the entire domain as one large regular CPM—when possible—is reduced by the fact that the global nature of the shape functions (particularly in the case of Lagrange and Bernstein polynomials) generally leads to fully populated matrices. As a result, when the number of boundary nodes increases, the computer time consumed for the domain integration of the stiffness and mass matrices may become higher than that required in the conventional FEM, obviously if the number of boundary nodes is the same [13, 22]. Therefore, it becomes obvious that there is still a need for further improvement of the CPM method. For this purpose, this paper investigates the possibility of replacing the Galerkin/Ritz formulation by a *global collocation* scheme.

The collocation method is one of the most competitive numerical methods for solving differential equations. Basically, a collocation method involves the determination of an appropriate solution in a suitable set of functions, sometimes called trial functions, by requiring the approximate solution to satisfy the boundary conditions and the differential equation at certain points, called the collocation points [27]. It has been found that using spline curves, or piecewise polynomials, is more effective in representing the solution to the differential equation than pure polynomials [28, p. 22]. The volume of Ascher *et al.* [29] provides a treatise on spline bases, collocation theory, and spline collocation for application to the numerical solution of BVP for ordinary differential equations. Fairweather and Meade [27] give an extensive review (273 papers covering the period 1934–1989) of collocation methods and various implementations that have been used. They describe the most common forms of collocation, including nodal, orthogonal, and collocation/Galerkin.

DOI: 10.1002/nme

Spline collocation methods are said to be more efficient than collocation/Galerkin methods and Galerkin methods. There are a number of choices to be made when applying spline collocation to approximate solutions of differential equations. These include the particular spline basis to use (Hermite, B-spline, etc.), the order of the spline function to use, the regularity of the spline curve to employ, and the locations of the collocation points. The relevant investigation continues until today, for example [30–33].

Concerning nonrectangular domains, Van Blerk and Botha [34] showed that the approximation of derivatives $(\partial u/\partial x, \partial u/\partial y)$, and particularly the cross-derivative term $(\partial^2 u/\partial x \partial y)$, could be improved by transforming the full domain rather than the individual elements; for this purpose they applied the transfinite interpolation [35, 36]. However, it should be strongly emphasized that in [34] both the domain and the partial differential equation (PDE) were transformed while the solution was approximated through the tensor product of Hermitian interpolation polynomials, thus requiring four degrees of freedom (DOFs) per node. In addition, within the last decade some advanced meshfree/meshless collocation methods using radial basis functions have appeared [37–42].

It is worth mentioning that if the basis functions are particular solutions of the differential equation then only the boundary conditions need to be satisfied. This is called the collocation Trefftz method (CTM) [6], which is also referred to as the indirect Trefftz method in [43], or the boundary solution procedure in [44]. The latest review paper is probably due to Li *et al.* [7].

Within this context, as already mentioned, this paper proposes a new approach of the previous CPM method in conjunction with the collocation method. Since the equation matrices do not require any domain integration effort, the proposed approach is called '*integration-free* Coons macroelement' or, equivalently, 'Coons-patch collocation' (CPC) method. The main novel feature of the CPC method is the replacement of the Galerkin/Ritz formulation with a collocation formulation while preserving the same high order cardinal global shape functions with the CPM method. Concerning potential problems, a second characteristic is the use of *only one* DOF per node, instead of four DOFs, as commonly used in several schemes that are based on global Hermitian interpolation in the entire domain or only near the boundary. It is also clarified that the CPC method, when compared to the CPM method, preserves the capability of coupling adjacent macroelements using compatibility and equilibrium conditions. The performance of this method is studied in 2D Poisson and Laplace test cases.

2. THE PROPOSED GLOBAL COLLOCATION METHOD

2.1. General

The proposed methodology is discussed using the Poisson PDE:

$$\nabla^2 u = f \quad \text{in } \Omega \tag{1}$$

where $u = u(x, y)$ denotes the unknown function (potential), ∇ is the operator del, and $f = f(x, y)$ is a known forcing function in Cartesian coordinates x and y.

DOI: 10.1002/nme

We shall seek an approximate solution to (1) that is a linear combination of the shape functions $\{\psi_i(x, y)\}$, $i = 1, 2, \ldots, N$:

$$\tilde{u}(x, y) = \sum_{i=1}^{N} u_i \psi_i(x, y) \tag{2}$$

where the unknown nodal potentials u_j are to be determined.

Generally, the shape functions possess the rigid body property and allow for an isoparametric mapping:

$$\sum_{i=1}^{N} \psi_i(x, y) = 1, \quad \sum_{i=1}^{N} x_i \psi_i(x, y) = x \quad \text{and} \quad \sum_{i=1}^{N} y_i \psi_i(x, y) = y \tag{3}$$

Among several alternatives, this paper proposes the use of global and cardinal shape functions $\psi_i(x, y)$, which are based on Coons (boundary-only) or Coons–Gordon transfinite interpolation [35, 36]. According to previous reports [19–26], $\psi_i(x, y)$ are produced by considering a unit square A′B′C′D′ (with normalized coordinates, $0 \leqslant \xi, \eta \leqslant 1$), that is mapped into the curvilinear quadrilateral domain ABCD $\equiv \Omega$ (with Cartesian coordinates xy). In case of a regular geometry, Equation (2) is obtained for the entire problem domain Ω. In contrast, the domain is subdivided into a small number of regular subdomains. In general, the interpolation of the potential within every subdomain is of the form:

$$\tilde{u}(\xi, \eta) = A_\xi(u) + A_\eta(u) - A_{\xi\eta}(u) \tag{4}$$

where A_ξ, A_η, and $A_{\xi\eta}$ are projections (lofting operators) previously described in [23]. For the completeness of the text, a summary is given in Appendix A.

The expression (4) is quite general and includes two broad categories of shape functions. The first category is the '*boundary-only Coons interpolation*', in which the three projections A_ξ, A_η, and $A_{\xi\eta}$ refer to boundary nodes only; this interpolation is successfully applicable to only a few number of problems. The second category is the '*transfinite Coons–Gordon interpolation*', in which internal nodes are considered as well. In both categories, each of the single-variable functions along the boundary, i.e. $u(\xi, 0)$, $u(1, \eta)$, $u(\xi, 1)$, and $u(0, \eta)$ is approximated in a standard way, for example in terms of piecewise-linear (hat functions), cubic B-splines, or Lagrange polynomials. Therefore, closed-form cardinal global shape functions $\psi_i(x, y)$ are automatically derived. Details can be found in [22–24].

2.2. Boundary conditions and discretization

In the general case, there are three types of boundary conditions: Dirichlet (essential), Neumann (natural), and Robin (mixed). For the sake of brevity, the third case is not considered in this paper. Therefore, the boundary $\Gamma = \Gamma_1 + \Gamma_2$ consists of the following:

(a) essential conditions, such as $u = \bar{u}$ on Γ_1;
(b) natural conditions of the type $\partial u/\partial n = \bar{q}$ on Γ_2.

In the sequence, let us assume that the boundary consists of $N_\Gamma = N_\mathrm{D} + N_\mathrm{N}$ boundary nodes; essential (Dirichlet) and natural (Neumann) boundary conditions are assigned to N_D and N_N nodes, respectively. In the general case, N_I internal nodes also exist.

DOI: 10.1002/nme

Following previous experience [27, 29], the proposed CPC methodology consists of two steps. The first concerns the collocation of the boundary conditions while the second concerns the collocation (fulfilment) of the PDE.

2.3. Collocation for the boundary conditions

Taking the normal derivative of (2), the general expression for the flux is obtained:

$$q=\frac{\partial\tilde{u}}{\partial n}=\sum_{j=1}^{N}\left[\frac{\psi_j(x,y)}{\partial n}\right]u_j \tag{5}$$

where $N=N_\Gamma+N_\mathrm{I}$ is the total number of nodes.

The application of (5) at all N_N Neumann nodes leads to

$$\bar{\mathbf{q}}_\mathrm{N}=\mathbf{A}_\mathrm{ND}\bar{\mathbf{u}}_\mathrm{D}+\mathbf{A}_\mathrm{NN}\mathbf{u}_\mathrm{N}+\mathbf{A}_\mathrm{NI}\mathbf{u}_\mathrm{I} \tag{6}$$

where the subscripts 'N' and 'D' correspond to the Neumann and the Dirichlet parts of the boundary, respectively, while 'I' corresponds to the internal nodes. The matrices $\mathbf{A}_\mathrm{ND}(N_\mathrm{N}\times N_\mathrm{D})$, $\mathbf{A}_\mathrm{NN}(N_\mathrm{N}\times N_\mathrm{N})$, and $\mathbf{A}_\mathrm{NI}(N_\mathrm{N}\times N_\mathrm{I})$ consist of the normal derivatives, i.e. the elements $[A]_{ij}=\partial\psi_j(x_i,y_i)/\partial n$. Arranging (6) so that all prescribed boundary conditions are included on the right-hand side, one obtains:

$$[\mathbf{A}_\mathrm{NN}\ \ \mathbf{A}_\mathrm{NI}]\cdot\begin{bmatrix}\mathbf{u}_\mathrm{N}\\ \mathbf{u}_\mathrm{I}\end{bmatrix}=\bar{\mathbf{q}}_\mathrm{N}-\mathbf{A}_\mathrm{ND}\bar{\mathbf{u}}_\mathrm{D} \tag{7}$$

2.4. Collocation for the PDE

Collocation of (1) at all N_I internal nodes (or at an equal number of internal points) leads to

$$[\mathbf{A}_2^\mathrm{D}\ \ \mathbf{A}_2^\mathrm{N}\ \ \mathbf{A}_2^\mathrm{I}]\cdot\begin{bmatrix}\bar{\mathbf{u}}_\mathrm{D}\\ \mathbf{u}_\mathrm{N}\\ \mathbf{u}_\mathrm{I}\end{bmatrix}=[\mathbf{f}] \tag{8}$$

where the matrices $\mathbf{A}_2^\mathrm{D}$ $(N_\mathrm{I}\times N_\mathrm{D})$, $\mathbf{A}_2^\mathrm{N}$ $(N_\mathrm{I}\times N_\mathrm{N})$, and $\mathbf{A}_2^\mathrm{I}$ $(N_\mathrm{I}\times N_\mathrm{I})$ consist of elements given as

$$[A_2]_{ij}=\nabla^2\psi_j(x_i,y_i)=\frac{\partial^2\psi_j(x_i,y_i)}{\partial x^2}+\frac{\partial^2\psi_j(x_i,y_i)}{\partial y^2} \tag{9}$$

and the vector $\mathbf{f}$ consists of the known values $f(x_i,y_i)$. In (8,9), the subscript '2' in A_2 stands for the second derivatives involved in the Laplacian; for an arbitrary curvilinear patch these are given by

$$\begin{aligned}
\frac{\partial^2\psi_j}{\partial x^2}&=\left(\frac{\partial\xi}{\partial x}\right)^2\frac{\partial^2\psi_j}{\partial\xi^2}+2\frac{\partial\xi}{\partial x}\frac{\partial\eta}{\partial x}\frac{\partial^2\psi_j}{\partial\xi\partial\eta}+\left(\frac{\partial\eta}{\partial x}\right)^2\frac{\partial^2\psi_j}{\partial\eta^2}+\frac{\partial^2\xi}{\partial x^2}\frac{\partial\psi_j}{\partial\xi}+\frac{\partial^2\eta}{\partial x^2}\frac{\partial\psi_j}{\partial\eta}\\
\frac{\partial^2\psi_j}{\partial y^2}&=\left(\frac{\partial\xi}{\partial y}\right)^2\frac{\partial^2\psi_j}{\partial\xi^2}+2\frac{\partial\xi}{\partial y}\frac{\partial\eta}{\partial y}\frac{\partial^2\psi_j}{\partial\xi\partial\eta}+\left(\frac{\partial\eta}{\partial y}\right)^2\frac{\partial^2\psi_j}{\partial\eta^2}+\frac{\partial^2\xi}{\partial y^2}\frac{\partial\psi_j}{\partial\xi}+\frac{\partial^2\eta}{\partial y^2}\frac{\partial\psi_j}{\partial\eta}
\end{aligned} \tag{10}$$

DOI: 10.1002/nme

where the quantities related to the inverse of Jacobian matrix, such as $\partial\xi/\partial x$, etc., are calculated as usual [2, p. 190].

Furthermore, by combining (7) and (8) one obtains the final algebraic system:

$$\begin{bmatrix} \mathbf{A}_{\mathrm{NN}} & \mathbf{A}_{\mathrm{NI}} \\ \mathbf{A}_2^{\mathrm{N}} & \mathbf{A}_2^{\mathrm{I}} \end{bmatrix} \cdot \begin{bmatrix} \mathbf{u}_{\mathrm{N}} \\ \mathbf{u}_{\mathrm{I}} \end{bmatrix} = \begin{bmatrix} \bar{\mathbf{q}}_{\mathrm{N}} - \mathbf{A}_{\mathrm{ND}} \cdot \bar{\mathbf{u}}_D \\ -\mathbf{A}_2^{\mathrm{D}} \cdot \bar{\mathbf{u}}_{\mathrm{D}} \end{bmatrix} \tag{11}$$

which consists of $(N_{\mathrm{N}}+N_{\mathrm{I}})$ equations with $(N_{\mathrm{N}}+N_{\mathrm{I}})$ unknowns.

2.5. *Coupling of adjacent macroelements*

In domains of complicated shape, a safe approach is to split them into regular convex macroelements (subregions). Then, for each macroelement the matrix appearing on the left side of Equation (11) is written. The assembly of these matrices is performed by imposing compatibility and equilibrium conditions at the interface nodes, similar to the conventional FEM procedure. Thus, the unknown flux along the interface is temporarily eliminated, and is calculated after the unknown potentials of every macroelement have been determined.

3. NUMERICAL EXAMPLES

The proposed CPC methodology is demonstrated through five examples in which the numerical solutions are compared to the previous CPM method [22–24], the conventional finite element (FEM) solution, and closed-form analytical expressions. Numerical results were obtained using a PC with Intel Pentium III processor-450 MHz and 256 MB of RAM.

When referring to comparisons with the FEM, we mean bilinear (four-node) finite elements [2] with a mesh that is characterized by the *same* number and location of nodes used in both the CPC and CPM solutions. For a reliable estimation of the solution quality, two error norms of normalized energy type are introduced as follows:

$$L_u = \frac{\sqrt{\int_\Omega (u_{\mathrm{calculated}} - u_{\mathrm{exact}})^2 \, \mathrm{d}\Omega}}{\sqrt{\int_\Omega (u_{\mathrm{exact}})^2 \, \mathrm{d}\Omega}} \tag{12a}$$

$$L_q = \frac{\sqrt{\int_\Omega (\mathbf{q}_{\mathrm{calculated}} - \mathbf{q}_{\mathrm{exact}})^{\mathrm{T}} (\mathbf{q}_{\mathrm{calculated}} - \mathbf{q}_{\mathrm{exact}}) \, \mathrm{d}\Omega}}{\sqrt{\int_\Omega (\mathbf{q}_{\mathrm{exact}})^{\mathrm{T}} (\mathbf{q}_{\mathrm{exact}}) \, \mathrm{d}\Omega}} \tag{12b}$$

where $u_{\mathrm{calculated}}$ and u_{exact} are the approximate and exact values of the potential at point $\mathbf{x}$, while $\mathbf{q}_{\mathrm{calculated}}$ and $\mathbf{q}_{\mathrm{exact}}$ are the approximate and exact values of the flux vector ($\mathbf{q} = [\partial u/\partial x \;\; \partial u/\partial y]^{\mathrm{T}}$) at point $\mathbf{x}$.

The abovementioned error norms are measures for the overall accuracy of the numerical solution. It is clarified that all subsequent figures relevant to the error norm L_u are illustrated in doubly logarithmic graphs and strictly refer to (12a). On the contrary, the subsequent tables include both error norms in a per cent (%) format.

For the sake of brevity, in all examples the potential along each of the four sides of each Coons patch has been interpolated using only Lagrange polynomials.

DOI: 10.1002/nme

Example 1: *Steady-state conduction in a cylindrical wall*. This example was taken from the collocation literature [45]; it also served for the evaluation of the CPM approach [24]. It refers to the potential problem (Laplace equation) with a 'steep' temperature distribution, appearing along the radius of a thick, long, hollow cylinder. The latter is subjected to a given uniform inner surface temperature ($T_1=1000°C$) and a given uniform outer surface temperature ($T_2=0°C$) while the inner and outer radii are $R_1=1$ and $R_2=32$, respectively. The analytical temperature distribution depends on the radial direction only, and is given by [46]:

$$T(r)=T_1+\frac{(T_2-T_1)}{\ln(R_2/R_1)}\ln(r/R_1) \tag{13}$$

Due to the radial symmetry of the problem, we deal only with an annular circular part of 45° as shown in Figure 1(a). Each one of the two circumferential arcs (BC and DA) is uniformly divided into $m=4$ segments. Each one of the radial sides (AB and CD) is uniformly divided into a variable number of $n=4$ up to $n=18$ segments; the case $n=10$ is shown in Figure 1(a). Moreover, the remaining three radii passing through the nodes along the sides AD and BC are discretized in a similar way. Clearly, all models (CPC, CPM, and FEM) share the same mesh shown in Figure 1(b).

The first step in implementing Equation (11), as described by (7), is to apply the Neumann boundary conditions at the $N_r=2(n-1)$ nodes along sides AB and CD shown in Figure 1(a). For the second step of implementing Equation (11), as described by (8), the choices tested concerning the location of the collocation points are outlined below.

First, the PDE was fulfilled at all the $N_I=(m-1)(n-1)$ internal nodes (nodal collocation). Figure 2(a) depicts that the corresponding CPC solution (CPC-node) leads to a better overall solution than FEM but worse than CPM.

In the sequel, the PDE was fulfilled at the mid-points of the radial segments along AB and CD ($N'_I=mn=4n$ points in total). Figure 2(a) shows that the error of the CPC solution (CPC-mid) significantly decreases and is comparable to the quality of the CPM solution. Only in this particular

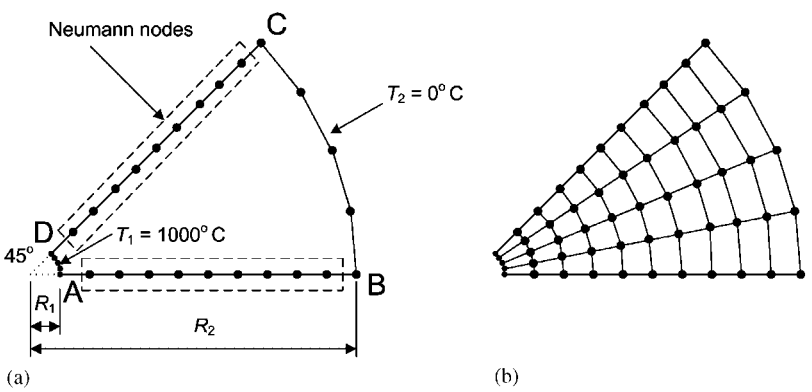

Figure 1. Example 1: annular segment of a cross-section in a thick-walled cylinder ($R_1=1$, $R_2=32$) of infinite length using: (a) collocation at the Neumann nodes denoted within the two dotted frames and (b) FEM model.

DOI: 10.1002/nme

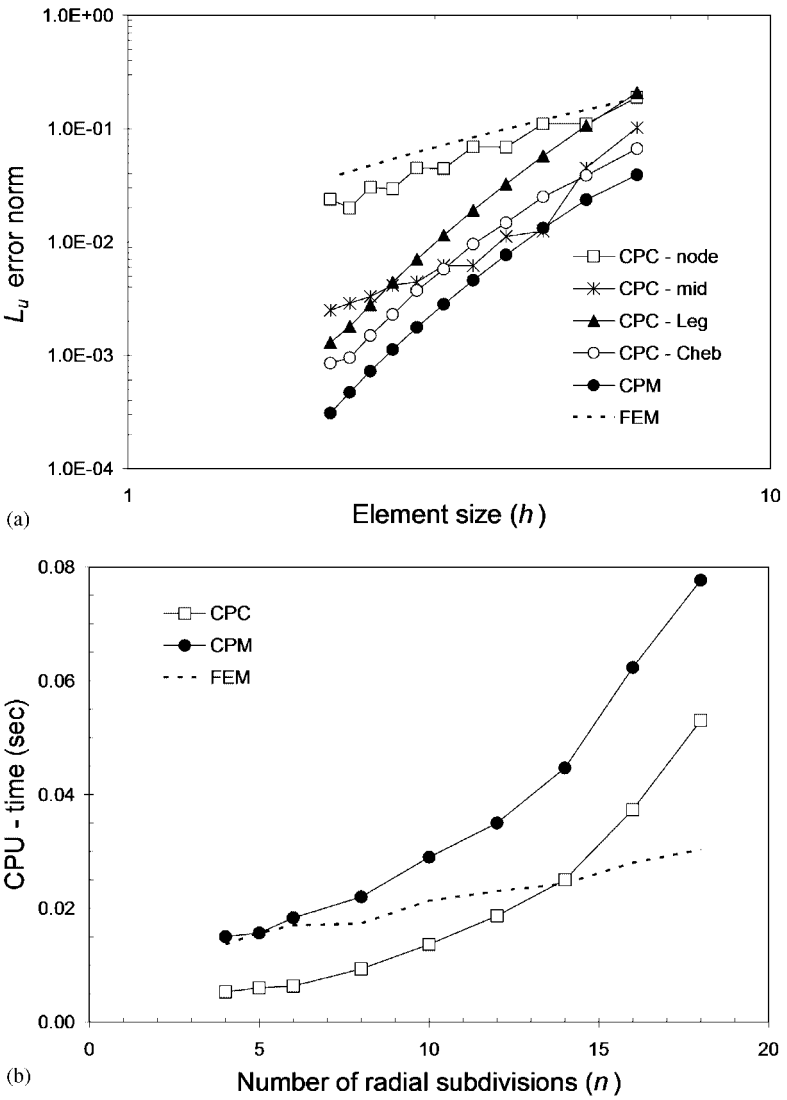

Figure 2. Example 1: annular segment: (a) L_u error norm versus radial element size (h), using the proposed Coons-patch collocation (CPC) method for several locations of the collocation points (CPC-node: nodal, CPC-mid: midpoint, CPC-leg: Legendre roots, and CPC-cheb: Chebyshev roots), the Coons-patch macroelement (CPM) method and the conventional FEM solution and (b) required CPU-time (s) as a function of increasing number of radial subdivisions (n).

case, a least-squares procedure is required because the number of equations becomes larger than the number nodes with unknown temperature.

In addition, the PDE was fulfilled at the roots of Legendre polynomials (Gaussian points, orthogonal collocation). The error norm (CPC-leg) was found to be between the two obtained using nodal (CPC-node) and mid-point collocation (CPC-mid). Figure 2(a) shows that the overall

DOI: 10.1002/nme

best CPC solution is rather the one based on the roots of Chebyshev polynomials of the second kind (CPC-cheb).

Finally, with respect to the CPU-time required, Figure 2(b) shows that the proposed CPC technique is always more efficient than the previously established CPM method. In more detail, for small values of radial subdivisions, such as $n=4$, the proposed CPC is faster than its preceding CPM method by a factor of 2.8 while for higher ones, such as $n=16$, this factor monotonically decreases to 1.7. In addition, for $n=4$ radial subdivisions, the proposed CPC method is 2.6 times faster than the conventional FEM and this advantage monotonically decreases to equal CPU-times (breakeven point) around $n=14$. For values higher than $n=14$, CPC becomes more time-consuming than the FEM; however, an essential convergence has been earlier achieved as shown in Figure 2(a).

Example 2: *Rectangular plate*. This example refers to a fully 2D potential problem concerning a rectangular plate of dimensions $L\times b=2\times 1$, with Dirichlet boundary conditions: $u=U_m\cos(\pi x/L)$ at the top side and $u=0$ elsewhere (Figure 3(a)). Due to the symmetry with respect to the y-axis, only the half right (hatched) part is discretized so that the domain becomes a unit square. The exact solution is given by [46]

$$u(x,y)=U_m[\sinh(\pi y/L)/\sinh(\pi b/L)]\cos(\pi x/L) \tag{14}$$

Each side of the unit square is uniformly divided into n segments thus including $(n-1)$ Neumann nodes along the boundary.

In the framework of the CPM method, it was found that, for this problem, convergence was achieved only when internal nodes were used [24]. Therefore, a uniform mesh of $N_I=(n-1)\times(n-1)$ internal nodes was initially used to test the limits of the proposed CPC method. These nodes control the global shape functions and are also the collocation points where the PDE is fulfilled (nodal collocation); as an alternative, the roots of either Legendre or Chebyshev polynomials can

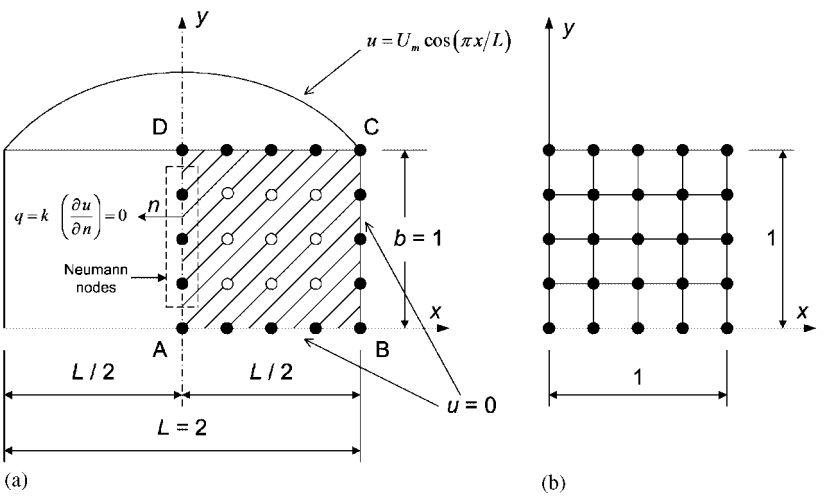

Figure 3. Example 2: rectangular plate analysed within the hatched square domain using: (a) Coons collocation method with boundary nodes (black-filled circles) and internal nodes (white-filled circles), as well as and (b) FEM model.

DOI: 10.1002/nme

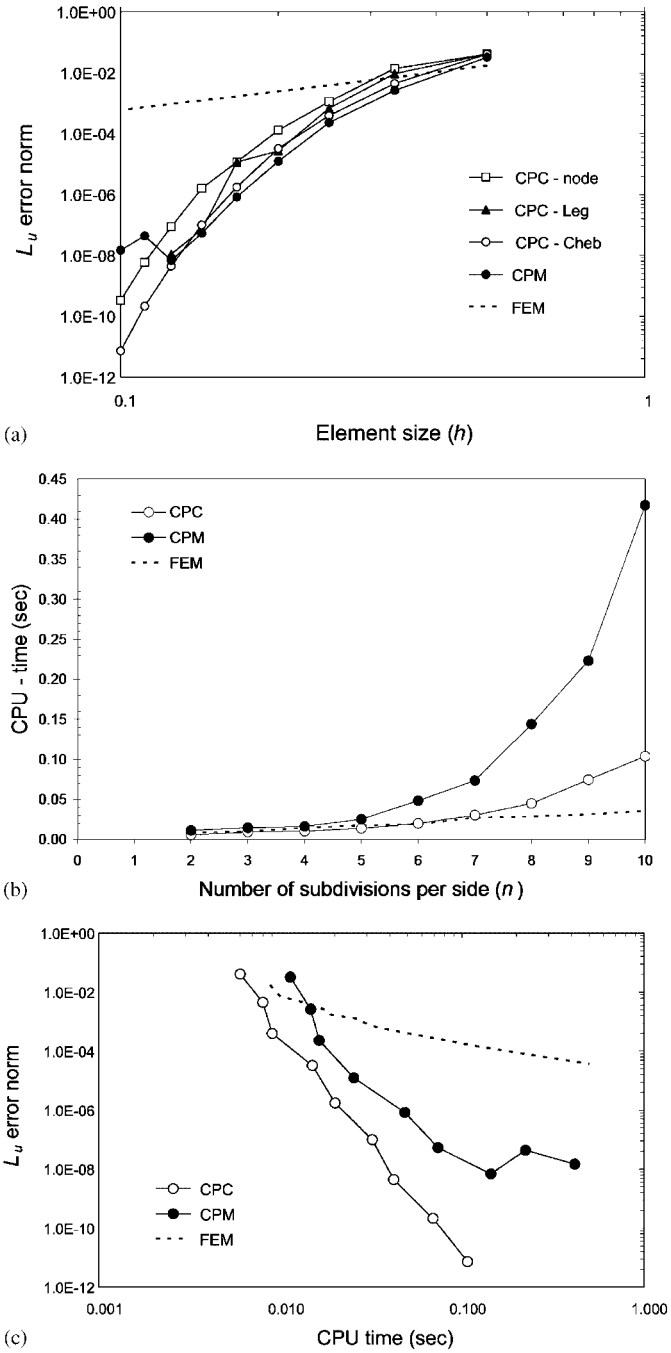

Figure 4. Example 2: rectangular plate: (a) L_u error norm versus element size (h); (b) CPU-time versus discretization; and (c) L_u error norm versus CPU-time, using the proposed Coons-patch collocation (CPC) method, Coons-patch macroelement (CPM) method, and the conventional finite element (FEM) model.

DOI: 10.1002/nme

be chosen (orthogonal collocation). Note that in Figure 4(a) both the CPC and CPM formulations converge very fast even for a small number of boundary nodes and become superior to the low-degree (four-node) conventional finite elements. It should be clarified that, as in [24], for this particular case of uniform mesh, the CPM formulation coincides with the traditional Lagrange-type finite element.

With respect to the required CPU-time, Figure 4(b) shows that the computational cost for the CPM method is higher than that of the conventional FEM, while for a certain level of the L_2 error norm, the proposed CPC is the most computationally efficient technique tested in this paper, as depicted in Figure 4(c).

Finally, it was found that for a given boundary discretization (n subdivisions per side), in order to apply the proposed Coons-patch methods (either CPM or CPC) it is not necessary to use the same mesh density and the same locations for the internal nodes (as required in traditional Lagrange-type finite elements). It is clearly given in Table I that only one node in the centre of the domain significantly decreases the L_u error norm (from 18.1 to 3.7%) when the proposed CPC method is applied. Furthermore, by increasing the number of internal nodes to 4 (in a uniform equidistant 2×2 arrangement), the L_u error norm converges to a value near 1.4%, and progressively decreases to negligible errors. To each row of a certain n-value in Table I, the corresponding error norm denoted in bold (within shadowed cells) corresponds to such an arrangement of the internal nodes so that they correspond to the conventional Lagrange-type finite element; it may be noted that no essential error reduction is achieved when exceeding this critical number of internal nodes.

Example 3: *Nonrectangular quadrilateral under Dirichlet boundary conditions*. This example was taken from collocation literature [34], and illustrates the behaviour of the proposed collocation method in an adequately distorted nonrectangular quadrilateral ABCD as shown in Figure 5(a). The forcing function $f(x, y)$ (cf. Equation (1)) was chosen as $f(x, y)=-(x^2+y^2)+3xy-50x-350y+15\,000$. Choosing homogeneous Dirichlet boundary conditions [34]:

$$u(x,0)=0 \quad (0\leqslant x\leqslant 100), \quad u(x,75-x/2)=0 \quad (50\leqslant x\leqslant 100)$$

$$u(x,y=x)=0 \quad (0\leqslant y\leqslant 50), \quad u(100,y)=0 \quad (0\leqslant y\leqslant 25)$$

the exact solution is given by

$$u(x,y)=y(x-100)(y-x)(y+x/2-75) \tag{15}$$

Each side of the quadrilateral was uniformly divided into $n=2$, 3, 4, and 5 segments, while a uniform mesh of $N_{\mathrm{I}}=(n-1)\times(n-1)$ internal nodes was used to investigate the convergence of the method. The solution quality is shown in Figure 5(b), where it can be noted that even for $n=4$ (the discretization shown in Figure 5(a)) the CPC solution coincides with the analytical values. In comparison with the Hermitian-based collocation method of Reference [34], the proposed CPC method is far superior because it presents a *zero* error over the *entire* domain even for $n=4$ subdivisions, which is the most coarse available mesh in [34]; the same superiority appears in the fluxes, as well.

Example 4: *Torsion of a bar with an elliptic cross-section*. This example serves to show the applicability of the CPC method in fully curvilinear domains where no straight line segment appears. The typical equation of torsion of a prismatic bar is given by

$$\nabla^2\Psi=-2G\tilde{\theta} \tag{16}$$

DOI: 10.1002/nme

Table I. Example 2 (L_u error norm, in %, of the calculated potential using the proposed CPC method for several uniform discretizations, n, along each side and a variable number of internal nodes, $N_I = n_x \times n_y$, uniformly distributed in the interior of the square domain).

		L_u error norm (in %)									
Number of subdivisions per side (n)	Boundary nodes only ($4n$)	Plus 1 internal node (1×1)	Plus 4 internal nodes (2×2)	Plus 9 internal nodes (3×3)	Plus 16 internal nodes (4×4)	Plus 25 internal nodes (5×5)	Plus 36 internal nodes (6×6)	Plus 49 internal nodes (7×7)	Plus 64 internal nodes (8×8)	Plus 81 internal nodes (9×9)	Plus 100 internal nodes (10×10)
2	8.2570	**4.0752**	1.8588	1.5861E+0	1.5052E+0	1.4808E+0	1.4758E+0	1.4730E+0	1.4723E+0	1.4720E+0	1.4718E+0
3	21.2808	3.8625	**1.3829**	3.0885E−1	1.8600E−1	1.4238E−1	1.4056E−1	1.4170E−1	1.4302E−1	1.4400E−1	1.4409E−1
4	18.4581	3.7566	1.3611	**1.1297E−1**	1.4515E−2	1.4702E−2	1.0462E−2	1.0637E−2	1.0572E−2	1.065EE−2	1.0767E−2
5	18.0802	3.7473	1.3618	1.1208E−1	**1.3010E−2**	1.7606E−3	5.9598E−4	4.3099E−4	4.4634E−4	4.3784E−4	4.4070E−4
6	18.1234	3.7485	1.3621	1.1190E−1	1.2956E−2	**1.1712E−3**	1.0349E−4	4.7145E−5	3.4822E−5	3.4429E−5	3.4575E−5
7	18.1272	3.7486	1.3622	1.1191E−1	1.2979E−2	1.1716E−3	**1.6027E−4**	1.6396E−5	6.3224E−6	2.6737E−6	2.4901E−6
8	18.1269	3.7486	1.3622	1.1191E−1	1.2978E−2	1.1703E−3	1.6011E−4	**8.5952E−6**	4.4479E−7	3.4237E−7	1.4467E−7
9	18.1269	3.7486	1.3622	1.1191E−1	1.2978E−2	1.1702E−3	1.6021E−4	8.5979E−6	**5.9082E−7**	2.6737E−6	1.0571E−8
10	18.1269	3.7486	1.3622	1.1191E−1	1.2978E−2	1.1702E−3	1.6021E−4	8.5925E−6	5.9045E−7	**3.2432E−8**	6.8527E−9
11	18.1269	3.7486	1.3622	1.1191E−1	1.2978E−2	1.1703E−3	1.6021E−4	8.5924E−6	5.9077E−7	3.0731E−8	**5.9204E−8**

DOI: 10.1002/nme

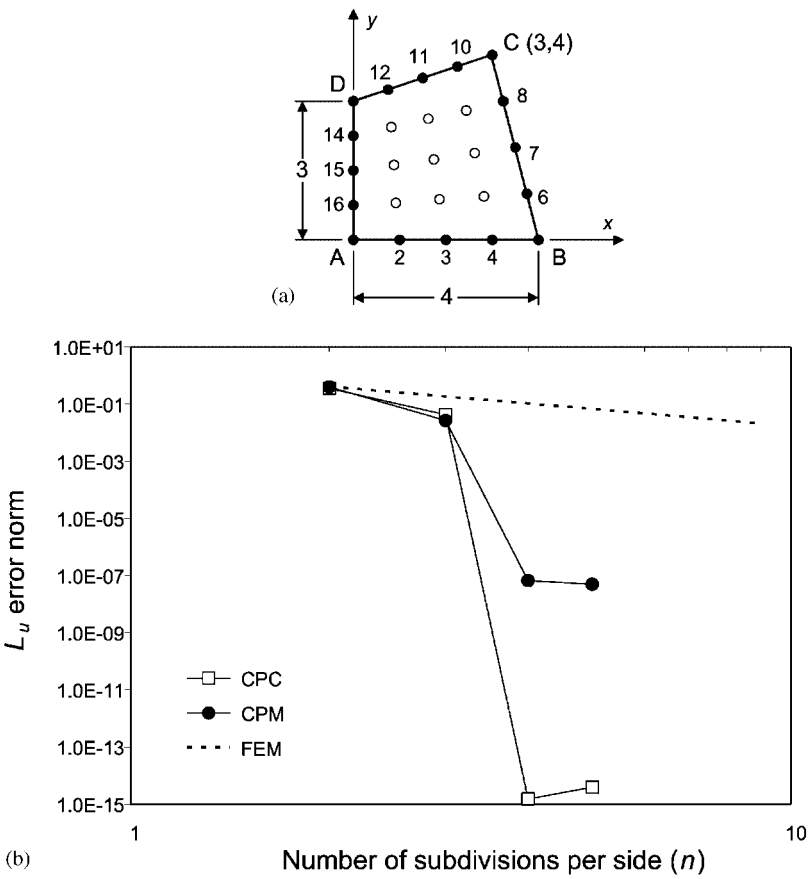

Figure 5. Example 3: nonrectangular quadrilateral under Dirichlet boundary conditions: (a) geometry and discretization and (b) L_u error norm versus number of subdivisions per side (n), using the proposed Coons-patch collocation (CPC) method in several variations (CPC-node: nodal, CPC-leg: Legendre roots, and CPC-cheb: Chebyshev roots), the Coons-patch macroelement (CPM) method, and the conventional FEM solution.

where $\Psi=\Psi(x,y)$ is the stress function, G the shear modulus, and $\tilde{\theta}$ the rate of twist, with the boundary condition $\Psi=0$ along the entire boundary.

For an elliptic cross-section the distribution of the stress function is given as

$$\Psi(x,y)=-\frac{G\tilde{\theta}}{2(a^{-2}+b^{-2})}\left(1-\frac{x^2}{a^2}-\frac{y^2}{b^2}\right) \tag{17}$$

where a and b are the semiaxes of the ellipse. Choosing the value of the constant $G\tilde{\theta}=1$ and the semiaxes $a=2$ and $b=1$, the problem to be solved is $\nabla^2\Psi=-2$ with $\Psi=0$ on Γ.

The boundary of the ellipse was discretized using $N_\Gamma=16$ and 32 boundary segments and $N_\mathrm{I}=(N_\Gamma/4-1)\times(N_\Gamma/4-1)$ internal nodes. Obviously, this situation corresponds to a single large

DOI: 10.1002/nme

isoparametric finite element of Lagrangian type. The results are presented in Table II where one may note that (i) convergence is achieved, and (ii) the nodal collocation is of adequate accuracy but orthogonal collocation (Gaussian and particularly Chebyshev points) is superior. One can also note that for both error norms, L_u and L_q, the difference between the Chebyshev-based CPC solution and the CPM solution is minor.

Example 5: *Potential flow past a cylinder*. The aim of this example is to depict that the proposed methodology is applicable to 2D domains that substantially differ from the reference square. It refers to the prediction of the potential infinite flow around a cylinder of unit radius ($a=1$).

In this case, the exact solution is analytically known and given by [47]

$$\Psi=\left(1-\frac{a^2}{r^2}\right)Ur\sin\theta \tag{18}$$

where Ψ denotes the stream function, U the flow velocity at infinity, and (r,θ) are the polar coordinates.

The solution domain is shown in Figure 6(a) and restricts to a strip of length $L=5\,\mathrm{m}$ and width $H=2\,\mathrm{m}$, while the infinite velocity was taken as $U=1\,\mathrm{m/s}$. The boundary conditions consist of the exact stream function Ψ along the entire boundary apart from the portion BC along which the radial velocity vanishes thus creating a Neumann type condition ($\partial\Psi/\partial x|_{\mathrm{BC}}=0$).

First, the external boundary of the domain was discretized using 26 nodes (Figure 6(a)). One can further notice that the side CD consists of two straight segments, i.e. CF and FD, respectively, a fact that significantly differentiates the current example from the four previous ones. Unfortunately, due to the abrupt edge at point F, it was not possible to interpolate the *xy*-coordinates of the side CD through a unique expression of a Lagrange polynomial of ninth degree. Thus, it was decided to subdivide the domain into two convex quadrilateral areas by drawing the internal line segment FE with three extra nodes along it, as shown in Figure 6(a). Therefore, the (AEFD) and the (EBCF) macroelements in Figure 6(a) consist of 16 and 18 nodes, respectively. In addition to the aforementioned boundary nodes, internal nodes were introduced to each macroelement, i.e. 9 and 12 nodes, of uniform arrangement (3×3) and (4×3), respectively (denoted by white circles

Table II. Example 4 (L_u and L_q error norms, in %, of the calculated potential and flux using the proposed CPC method, the previous CPM method, and the conventional FEM).

		L_u and L_q error norms (in %)				
		Proposed CPC method where the PDE is fulfilled at:				
Number of boundary subdivisions (N_Γ)	Error norm	Internal nodes*	Roots of Legendre polynomial†	Roots of Chebyshev polynomial of second kind†	CPM	FEM
16	$L_u\rightarrow$	1.081	0.830	0.520	0.506	11.046
	$L_q\rightarrow$	2.691	2.174	1.923	1.882	28.469
32	$L_u\rightarrow$	0.325	0.055	0.036	0.035	2.859
	$L_q\rightarrow$	1.490	0.416	0.388	0.380	14.224

*Nodal collocation.
†Orthogonal collocation.

DOI: 10.1002/nme

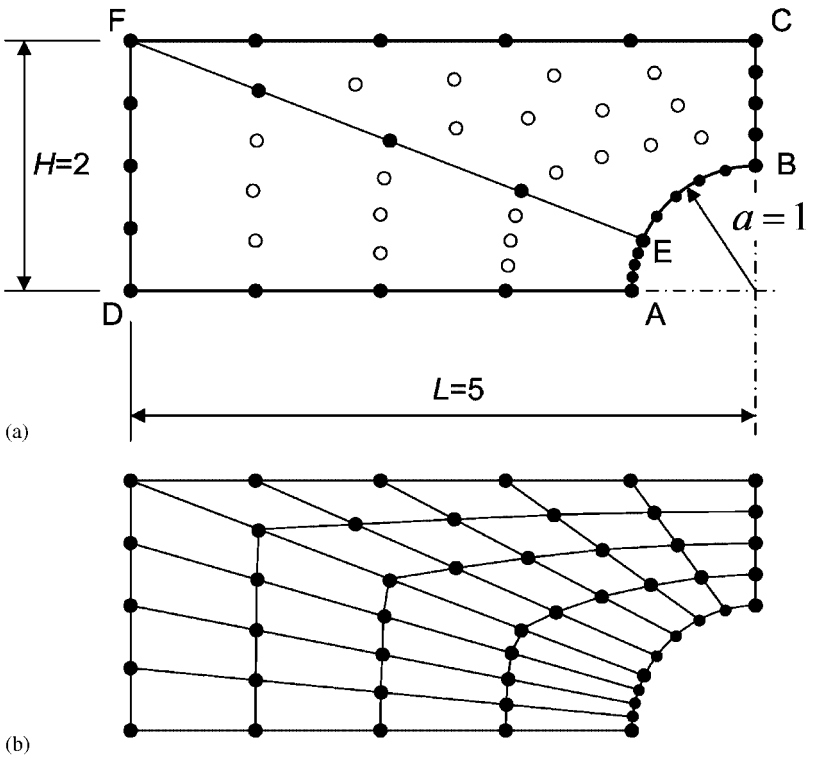

Figure 6. Example 5: potential flow past a cylinder using: (a) two Coons macroelements (50 nodes) and (b) 36 bilinear finite elements (50 nodes).

Table III. Example 5 (L_u and L_q error norms, in %, of the calculated potential and flux using the proposed CPC method, the previous CPM method, and the conventional FEM).

	L_u and L_q error norms (in %)				
	Proposed CPC method where the PDE is fulfilled at:				
Error norm	Internal nodes*	Roots of Legendre polynomial†	Roots of Chebyshev polynomial of second kind†	CPM	FEM
$L_u \rightarrow$	0.007	0.013	0.003	0.325	1.102
$L_q \rightarrow$	2.191	1.703	1.838	13.959	16.923

*Nodal collocation.
†Orthogonal collocation.

in Figure 6(a)). Table III represents that the L_u error norm was in favour of the proposed CPC method (0.003–0.013%), while for the CPM and the conventional FEM (36 bilinear elements, 50 nodes) this norm was found to be equal to 0.32 and 1.10%, respectively.

DOI: 10.1002/nme

4. DISCUSSION

4.1. General

The proposed CPC methodology is a higher order global collocation technique that has not only similarities but also differences from previous collocation techniques. In brief, neither the differential equation nor the boundary conditions are satisfied by the shape functions; therefore, according to the categorization by Finlayson [48, p. 11], the CPC approach should be classified as a *mixed* method.

The proposed CPC method is based on the same functions as those used previously in the transfinite CPM (Galerkin/Ritz) method. Since *only* Lagrange polynomials are used, the cardinal global shape functions are automatically constructed in terms of the position of the boundary and the internal nodes, *only*. Concerning the position of the collocation points, it was shown that CPC can be successfully implemented in either nodal or orthogonal form. In both cases, adequate accuracy was achieved taking the number of collocation points equal to the number of internal nodes. It should become clear that in case of orthogonal collocation, the aforementioned collocation points were implemented in a global manner within the entire domain. Concerning the fulfilment of the boundary conditions, in the case of boundary geometries that are not simple, if one uses the collocation method at the boundary in the same way as it is performed in the interior of the domain, demanding the residual to be equal to zero at certain points, the polynomial degree must be very large. An equally large degree of the trial function is demanded when the solution is not very smooth, for example, in the case of a crack or a boundary layer. While the aforementioned drawback characterizes all collocation methods, the proposed approach has the major advantage of using only one DOF, i.e. using only the potential u_j assigned to each node 'j', in opposition to previous Hermite spline methods which require the derivatives $\partial u_j/\partial x$, $\partial u_j/\partial y$, and $\partial^2 u_j/\partial x \partial y$ as well [34, 45]. In this way, the presence of only one-fourth of the previously required DOFs is now necessary. A precursor of the latter idea was recently introduced and successfully applied to 1D problems [49, 50].

Apart from the abovementioned Lagrange polynomials, a thorough investigation on the performance of the proposed CPC method should include all other interpolations previously used in the CPM, i.e. piecewise-linear and cubic B-splines, as well as others such as Bézier, higher order B-splines, and NURBS. It is remarkable that for all these interpolations there exists a compact support that leads to banded matrices, the Bézier interpolation being an exception. However, due to limited available space, the discussion restricts to the first two cases only. In brief, it was found that the piecewise-linear approximation has such a poor performance that it is not practically applicable. In addition, the *natural* cubic B-splines approximation (zero curvature at the ends of each side, as was author's choice in his previous CPM method [19, 24]) leads to better results but are significantly worse than those obtained using Lagrange polynomials. With respect to Example 1, it was found that it is not only the consideration of the curvatures (associated with additional DOF at the corners A, B, C, and D of the patch) but mainly the polynomial degree of B-spline that improves the quality of the results. However, the use of the abovementioned integration points, implemented in a global manner within the entire domain, in combination with cubic B-splines is not recommended because it is possible to have a lower number of integration points (Gauss, Chebyshev) within some knot intervals than required. Interestingly enough, this finding is consistent with analogous results obtained in [24, p. 334], where it was shown that a scheme of 2×2 Gauss points per integration cell was superior rather than implementing global Gaussian integration in the entire domain.

DOI: 10.1002/nme

4.2. Boundary-only approximation

Undoubtedly, there is only a reduced class of problems of which the numerical solution can be accurately approximated by the *boundary-only Coons interpolation*. For instance, since Example 1 is characterized by a radial symmetry, it could be alternatively solved using the boundary-only approximation and, consequently, using only the boundary nodes shown in Figure 1(a). Then, after the Neumann boundary conditions are considered (Equation (7)), the only modification in the standard transfinite formulation (Equation (11)) would be to reduce the collocation points along one arbitrary radius within the domain; of course, the boundaries AB or CD could be preferred. Therefore, since the fulfilment of the PDE creates additional equations that outnumber the Neumann boundary nodes, a least-squares procedure should be performed.

4.3. Transfinite approximation

In contrast to Section 4.2, the general BVP requires the use of the *transfinite Coons–Gordon interpolation* (Equation (A4)). In general, it is suggested to distribute the internal nodes uniformly within the domain, something that can be easily implemented in an automatic way. Without loss of generality, the standard procedure suggests that the PDE be fulfilled at the N_{I} internal nodes (nodal collocation) or at an equal number of internal points (orthogonal collocation: usually at the roots of the Legendre or the Chebyshev polynomial of the second kind), thus directly leading to a square matrix (left-hand-side matrix in Equation (11)). A more conservative approach could include the fulfilment of the PDE at more internal points, thus increasing the difference between the number of equations and the number of unknowns and requiring a least-squares solution.

4.4. Remarks on the examples

Further explanations and comments offering a better insight into the performance of the global basis functions, involved in both the proposed CPC and the previous CPM methods, are provided below.

Concerning Example 2, Table I presents that for polynomials up to the ninth degree the L_u error norm monotonically decreases, while it begins to increase for higher degrees, for which the full matrices are suspected to be ill-conditioned.

Concerning Example 3, it can be verified that the analytical solution (Equation (15)) in Cartesian coordinates includes the monomials $\{xy, y^2, xy^2, x^2y, y^3, x^3y, x^2y^2, xy^3\}$, of which x^2y^2 does not belong to the functional space of a Serendipity element. Moreover, considering the entire patch ABCD as a four-node bilinear element, it can be easily found that the relationship between the Cartesian and the normalized coordinates are: $x(\xi,\eta)=50(2\xi+\eta-\xi\eta)$ and $y(\xi,\eta)=25(2\eta-\xi\eta)$. As a result, the term $\xi^4\eta^4$ is the binomial of the highest degree that appears into the analytical solution. Therefore, a Lagrange polynomial at least of fourth degree would be sufficient to represent accurately the analytical solution, as occurred in the particular example.

Concerning Example 4, if the number of nodes is low then the transfinite interpolation is incapable of representing the exact solution accurately, although the latter includes only the terms x^2, y^2 and the constant. For example, when using $N_\Gamma=8$ boundary nodes plus one at the centre of the ellipse ($N_{\mathrm{I}}=1$), the functional space consists of all those monomials involved in the nine-node isoparametric finite element of Lagrangian type, thus also involving the terms ξ^2, η^2 and the constant. Obviously, the nonrectangular nature of the domain induces a non-linear relationship between the Cartesian (x, y) and the normalized (ξ,η) coordinates; thus reproducing the terms x^2

DOI: 10.1002/nme

and y^2 is not possible. In contrast, it is worth mentioning that Trefftz method in combination with the functional set $(x+\mathrm{i}y)^n$, with $\mathrm{i}^2=-1$, provides the exact solution to this problem [44].

4.5. A technical issue concerning CPU-time

The efficient calculation of the first and second derivatives ($\partial\psi_j/\partial\xi, \partial^2\psi_j/\partial\xi^2$, etc.) involved in the Laplacian terms (Equation (10)) could be alternatively performed in a more efficient way using divided differences (e.g. [28, pp. 1–8]). This fact would further improve the CPU-time performance of the proposed CPC method and would influence the results shown in Figures 2(b) and 4(b,c).

5. CONCLUSIONS

'Coons-Patch Macroelements' (CPM) have been previously proposed for the solution of engineering problems within quadrilateral domains; so far, they have been used mainly in conjunction with the finite element method. The novel feature of this work is that the Galerkin/Ritz formulation introduced initially in CPM was substituted by a global collocation method, retaining the same global shape functions, thus the term 'integration-free' Coons-patch macroelements is justified. From a limited number of examples, it is concluded that—probably due to the higher order approximation involved—the accuracy of the proposed technique was superior to the conventional FEM (for the same mesh density) and generally required lower computational cost for similar levels of accuracy (L_u and L_q error norms). However, it should be mentioned that, in complex geometries, the proposed method requires the subdivision of the domain into a small number of large, preferably convex, macroelements. In addition, domain decomposition is required when a singularity arises. As a rule-of-thumb, a number of no more than eight subdivisions per side of a Coons patch is suggested. It should be mentioned that in the five examples reported in this paper and in a variety of other examples under on-going investigation, no indication of numerical instability of the proposed method was noticed unless the degree of the approximating polynomial was higher than 9. So far the results are most encouraging and suggest that the proposed procedure can be successfully applied to a variety of engineering problems, such as wave propagation and elasto-dynamic problems, while the extension of the proposed method to 3D problems may become a most promising tool in engineering analysis.

APPENDIX A: TRANSFINITE COONS–GORDON INTERPOLATION FORMULAS

A.1. Boundary-only Coons interpolation

Let us assume that a 2D function $u(x, y)$ in a square $\Omega=(\mathrm{ABCD})$, with ξ and η denoting normalized coordinates ($0\leqslant\xi,\eta\leqslant1$), is known along the four sides of the boundary ($\xi=0,1;\ \eta=0,1$). In other words, the univariate functions $u(\xi,0), u(1,\eta), u(\xi,1)$, and $u(0,\eta)$ along the sides AB, BC, CD, and DA are known. Let us also consider the blending functions:

$$\begin{aligned} E_0(\xi) &= 1-\xi, \quad E_1(\xi)=\xi \\ E_0(\eta) &= 1-\eta, \quad E_1(\eta)=\eta \end{aligned} \tag{A1}$$

DOI: 10.1002/nme

In this case, Coons interpolation formula is given in terms of three projections ($\bar{A}_\xi, \bar{A}_\eta, \bar{A}_{\xi\eta}$) by

$$u(\xi,\eta)=\underbrace{E_0(\xi)u(0,\eta)+E_1(\xi)u(1,\eta)}_{\bar{A}_\xi}+\underbrace{E_0(\eta)u(\xi,0)+E_1(\eta)u(\xi,1)}_{\bar{A}_\eta}-\bar{A}_{\xi\eta}(\xi,\eta) \tag{A2}$$

where

$$\begin{aligned}\bar{A}_{\xi\eta}(\xi,\eta) &= E_0(\xi)E_0(\eta)u(0,0)+E_1(\xi)E_0(\eta)u(1,0)\\ &\quad +E_0(\xi)E_1(\eta)u(0,1)+E_1(\xi)E_1(\eta)u(1,1)\end{aligned} \tag{A3}$$

A.2. Transfinite Coons–Gordon interpolation

The transfinite Coons–Gordon interpolation is an enhancement of the Coons interpolation formula mentioned in Equations (A2), (A3); it includes both boundary and internal nodes, and it is given by a quite similar formula:

$$u(\xi,\eta)=A_\xi(u)+A_\eta(u)-A_{\xi\eta}(u) \tag{A4}$$

where A_ξ, A_η, and $A_{\xi\eta}$ are projections (lofting operators). In more details, we assume that the function $u(x, y)$ in a square $\Omega=$(ABCD) is known at lines $\xi=$constant and $\eta=$constant (Figure A1). These lines are $(n_\xi+1)$ ξ-lines vertical to the ξ-axis at the points: $[\boldsymbol{\xi}]=[\xi_0,\xi_1,\ldots,\xi_{n_\xi}]$, and $(n_\eta+1)$ η-lines vertical to the η-axis at the points: $[\boldsymbol{\eta}]=[\eta_0,\eta_1,\ldots,\eta_{n_\eta}]$.

Then, both the boundary and all the following functions are assumed to be known:

$$\begin{aligned}&u(\xi_i,\eta), \quad i=0,1,\ldots,n_\xi\\ &u(\xi,\eta_j), \quad j=0,1,\ldots,n_\eta\end{aligned} \tag{A5}$$

Let us further update the cardinal blending functions $E_i(\xi)$ for $i=0,1,\ldots,n_\xi$ ($\delta_{im}=$Kronecker delta):

$$E_i(\xi_m)=\delta_{im} \tag{A6}$$

where ξ_i and ξ_m being elements of $[\boldsymbol{\xi}]$. By analogy, we define cardinal blending functions $E_j(\eta)$ for $j=0,1,\ldots,n_\eta$.

Based on (A5) and (A6), the abovementioned unidirectional operators $A_\xi(u)$ and $A_\eta(u)$ are constructed as follows:

$$\begin{aligned}A_\xi(u) &= \sum_{i=1}^{n_\xi} u(\xi_i,\eta)\cdot E_i(\xi)\\ A_\eta(u) &= \sum_{j=1}^{n_\eta} u(\xi,\eta_j)\cdot E_j(\eta)\end{aligned} \tag{A7}$$

In the sequence, a 2D operator $A_{\xi\eta}(u)$, given by

$$A_{\xi\eta}(u)=A_\xi A_\eta(u)=\sum_{i=1}^{n_\xi}\sum_{j=1}^{n_\eta} u(\xi_i,\eta_j)\cdot E_i(\xi)\cdot E_j(\eta) \tag{A8}$$

can be constructed with the aid of the two unidirectional operators $A_\xi(u)$ and $A_\eta(u)$.

DOI: 10.1002/nme

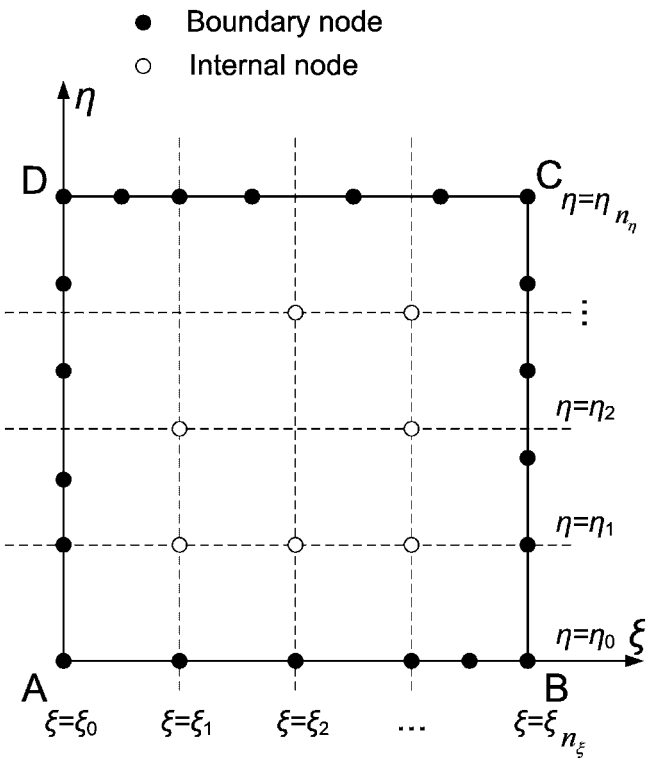

Figure A1. Transfinite reference patch (ABCD) composed of four curvilinear sides along the boundary ($\xi=0, 1$; $\eta=0, 1$), accompanied with several intermediate lines (inter-boundaries) of $\xi=$constant and $\eta=$constant.

A.3. Construction of global shape functions

Assuming the continuous functions existing in (A5), these are further interpolated using single-variable interpolants such as piecewise-linear, piecewise-quadratic, cubic B-splines, NURBS, Bernstein (Bézier), Lagrange polynomials, etc. Finally, when substituted in (A4), the global shape functions, $\psi_j(x, y)$, are derived. The interested reader may find in References [13–15, 19–22] closed-form expressions and illustrative graphs for the global shape functions obtained from this procedure. For example, for the intermediate node at $\xi=\xi_1$ along the side AB (Figure A1), the associated shape function is given by $\psi(\xi,\eta)=L_1^{(n_\xi)}(\xi)E_0(\eta)$, where $L_1^{(n_\xi)}(\xi)$ is the Lagrange polynomial of n_ξ-th degree, i.e. passing through $(n_\xi+1)$ points, $\xi_0, \xi_1, \ldots, \xi_{n_\xi}$, with $L_1^{(n_\xi)}(\xi_1)=1$.

A.4. Functional spaces

With respect to the $\xi\eta$-coordinate system, the boundary-only Coons interpolation creates a functional space that consists of the monomials $\{1, \xi, \xi^2, \ldots, \xi^{n_\xi}\}$ and $\{1, \eta, \eta^2, \ldots, \eta^{n_\eta}\}$, as well as the binomials $\{1, \xi, \xi^2, \ldots, \xi^{n_\xi}\}\cdot\eta$ and $\xi\cdot\{1, \eta, \eta^2, \ldots, \eta^{n_\eta}\}$. Obviously, in case of a rectangular domain the normalized coordinates (ξ, η) may be replaced by the Cartesian (x, y) ones, while in distorted

DOI: 10.1002/nme

domains the corresponding relationship generally becomes non-linear. Moreover, when the exact solution includes more terms than the aforementioned monomials and binomials, the transfinite interpolation becomes necessary.

REFERENCES

1. Ritz W. Über eine neue Methode zur Lösung gewisser Variations probleme der mathematischen Physik. *Zeitschrift für Reine und Angewandte Mathematik* 1909; **135**(1):1–61.
2. Zienkiewicz OC. *The Finite Element Method* (3rd edn). McGraw-Hill: London, 1977.
3. Wachspress E. *A Rational Finite Element Basis*. Academic Press: New York, 1975.
4. Malsch EA, Dasgupta G. Interpolations for temperature distributions: a method for all non-concave polygons. *International Journal of Solid and Structures* 2004; **41**:2165–2188.
5. Brebbia CA, Dominguez J. *Boundary Elements*: *An Introductory Course* (2nd edn). Computational Mechanics Publications: Southampton, 1992.
6. Kita E, Kamiya N. Trefftz method: an overview. *Advances in Engineering Software* 1995; **24**(1–3):3–12.
7. Li ZC, Lu TT, Huang HT, Cheng AHD. Trefftz, collocation, and other boundary methods—a comparison. *Numerical Methods for Partial Differential Equations* 2007; **23**:93–144.
8. Atluri SN. *The Meshless Method* (*MLPG*) *for Domain and BIE Discretizations*. Tech Science Press: Encino, 2004.
9. Liu GR. *Mesh Free Methods*: *Moving Beyond the Finite Element Method*. CRC Press: Boca Raton, 2003.
10. Schramm U, Pilkey WD. The coupling of geometric descriptions and finite element using NURBS—a study in shape optimization. *Finite Elements in Analysis and Design* 1993; **15**:11–34.
11. Hughes TJR, Cottrell JA, Bazilevs Y. Isogeometric analysis: CAD, finite elements, NURBS, exact geometry and mesh refinement. *Computer Methods in Applied Mechanics and Engineering* 2005; **194**:4135–4195.
12. Inoue K, Kikuchi Y, Masuyama T. A NURBS finite element method for product shape design. *Journal of Engineering Design* 2005; **16**(2):157–174.
13. Provatidis CG. Three-dimensional Coons macroelements: application to eigenvalue and scalar wave propagation problems. *International Journal for Numerical Methods in Engineering* 2006; **65**:111–134.
14. Provatidis C. Stress analysis of 3D solid structures using large boundary elements derived from 2D-Coons interpolation. In *Proceedings of ASME–Greek Section Conference*, Patras, Greece, Drakatos PA (ed.), 17–20 September 2001 (Paper ANG1/P129).
15. Provatidis C. Analysis of three-dimensional sound radiation problems using trimmed patch boundary elements. In *Proceedings 4th GRACM Congress on Computational Mechanics*, vol. I, Patras, Greece, Tsahalis DT (ed.), 27–29 June 2002; 402–409.
16. Farin G. *Curves and Surfaces for Computer Aided Geometric Design*: *A Practical Guide*. Academic Press: Boston, 1990.
17. Provatidis CG. Three-dimensional Coons macroelements in Laplace and acoustic problems. *Computers and Structures* 2005; **83**(4–5):1572–1583.
18. Provatidis CG. Analysis of box-like structures using 3-D Coons' interpolation. *Communications in Numerical Methods in Engineering* 2005; **21**(8):443–456.
19. Provatidis CG, Kanarachos AE. Performance of a macro-FEM approach using global interpolation (Coons') functions in axisymmetric potential problems. *Computers and Structures* 2001; **79**:1769–1779.
20. Provatidis CG. Coons-patch macroelements in potential Robin problems. *Forschung im Ingenieurwesen* 2002; **67**:19–26.
21. Provatidis CG. Analysis of axisymmetric structures using Coons' interpolation. *Finite Elements in Analysis and Design* 2003; **39**:535–558.
22. Provatidis CG. Coons-patch macroelements in two-dimensional eigenvalue and scalar wave propagation problems. *Computers and Structures* 2004; **82**(4–5):383–395.
23. Provatidis CG. Solution of two-dimensional Poisson problems in quadrilateral domains using transfinite Coons interpolation. *Communications in Numerical Methods in Engineering* 2004; **20**(7):521–533.
24. Provatidis CG. Coons-patch macroelements in two-dimensional parabolic problems. *Applied Mathematical Modelling* 2006; **30**(4):319–351.
25. Provatidis CG. Free vibration analysis of two-dimensional structures using Coons-patch macroelements. *Finite Elements in Analysis and Design* 2006; **42**(6):518–531.

DOI: 10.1002/nme

26. Provatidis CG. Transient elastodynamic analysis of two-dimensional structures using Coons-patch macroelements. *International Journal of Solids and Structures* 2006; **43**(22–23):6688–6706.
27. Fairweather G, Meade D. Survey of spline collocation methods for the numerical solution of differential equations. In *Mathematics for Large Scale Computing*, Diaz JC (ed.). Lecture Notes in Pure Applied Mathematics, vol. 120. Marcel Dekker: New York, 1989; 297–341.
28. De Boor C. *A Practical Guide to Splines*. Applied Mathematical Sciences, vol. 27. Springer: New York, 1978.
29. Ascher UM, Mattheij RMM, Russell RD. *Numerical Solutions of Boundary Value Problems for Ordinary Differential Equations* (2nd edn). SIAM: Philadelphia, PA, 1995.
30. Bialecki B, Fairweather G. Orthogonal spline collocation methods for partial differential equations. *Journal of Computational and Applied Mathematics* 2001; **128**(1–2):55–82.
31. Johnson RW. Higher order B-spline collocation at the Greville Absissae. *Applied Numerical Mathematics* 2005; **52**(1):63–75.
32. Liu X, Liu GR, Tai K, Lam KY. Radial point interpolation collocation method (RPICM) for the solution of nonlinear Poisson problems. *Computational Mechanics* 2005; **36**:298–306.
33. Jator S, Sinkala Z. A high order B-spline collocation method for linear boundary value problems. *Applied Mathematics and Computation* 2007; **191**:100–116.
34. Van Blerk JJ, Botha JF. Numerical solution of partial differential equations on curved domains by collocation. *Numerical Methods for Partial Differential Equations* 1993; **9**:357–371.
35. Gordon WJ, Hall CA. Transfinite element methods: blending-function interpolation over arbitrary curved element domains. *Numerische Mathematik* 1973; **21**:109–129.
36. Gordon WJ. Blending functions methods of bivariate multivariate interpolation and approximation. *SIAM Journal on Numerical Analysis* 1971; **8**:158–177.
37. Elansari M, Quazar D, Cheng AH-D. Boundary solution of Poisson's equation using radial basis function collocated on Gaussian quadrature nodes. *Communications in Numerical Methods in Engineering* 2001; **17**:455–464.
38. Liu GR, Wang JG. A point interpolation meshless method based on radial basis functions. *International Journal for Numerical Methods in Engineering* 2002; **54**:1623–1648.
39. Liszka TJ, Duarte CA, Tworzydlo WW. Hp-meshless cloud method. *Computer Methods in Applied Mechanics and Engineering* 1996; **139**:263–288.
40. Zhang X, Song KZ, Lu MW, Liu X. Meshless methods based on collocation with radial basis function. *Computational Mechanics* 2003; **30**:396–409.
41. Chen JT, Chang MH, Chen KH, Lin SR. The boundary collocation method with meshless concept for acoustic eigenanalysis of two-dimensional cavities using radial basis function. *Journal of Sound and Vibration* 2002; **257**(4):667–711.
42. Chen JT, Chang MH, Chen KH, Chen IL. Boundary collocation method for acoustic eigenanalysis of three-dimensional cavities using radial basis function. *Computational Mechanics* 2002; **29**:392–408.
43. Zienkiewicz OC, Kelly DW, Bettess P. The coupling of the finite element method and boundary solution procedures. *International Journal for Numerical Methods in Engineering* 1977; **11**(2):355–375.
44. Zielinski AP, Zienkiewicz OC. Generalized finite element analysis with T-complete boundary solution functions. *International Journal for Numerical Methods in Engineering* 1985; **21**:509–528.
45. Frind EO, Pinder GF. A collocation finite element method for potential problems in irregular domains. *International Journal for Numerical Methods in Engineering* 1979; **14**:681–701.
46. Carslaw HS, Jaeger JC. *Conduction of Heat in Solids*. Oxford University Press: London, 1959.
47. Karamcheti K. *Principles of Ideal-fluid Aerodynamics*, Krieger RE (ed.). Publishing Company: Huntington, New York, 1980; 383.
48. Finlayson BA. *The Method of Weighted Residuals and Variational Principles*. Academic Press: New York, 1972.
49. Provatidis CG. Free vibration analysis of elastic rods using global collocation. *Archive of Applied Mechanics* 2008; **78**(4):241–250.
50. Provatidis CG. Time- and frequency-domain analysis using lumped mass global collocation. *Archive of Applied Mechanics* (DOI: 10.1007/s00419-008-0203-z).

DOI: 10.1002/nme